Nuclear Physics B74 (1974) 189–210. North-Holland Publishing Company

INCLUSIVE PHOTOPRODUCTION OF PIONS, KAONS AND PROTONS AT 6 GeV

H. BURFEINDT, G. BUSCHHORN, H. GENZEL, P. HEIDE, U. KÖTZ, K.-H MESS, P. SCHMÜSER, B. SONNE, G. VOGEL and B.H. WIIK

Deutsches Elektronen-Synchrotron DESY, Hamburg, II. Institut für Experimentalphysik der Universität Hamburg, Max-Planck-Institut für Physik und Astrophysik, München

Received 12 December 1973
(Revised 13 February 1974)

Abstract: The invariant cross sections for inclusive photoproduction of charged pions, kaons and protons have been measured at DESY in the photon fragmentation region at a photon energy of 6 GeV. The π^+/π^- ratio is close to one at small values of the transverse momentum $p_\perp$ but increases with increasing values of $p_\perp$. This indicate that scaling is violated at large transverse momenta (or low missing masses). The same general behaviour is also observed in the K^+/K^- ratio, although here the ratio is significantly larger than one even at small transverse momenta. A comparison with preliminary data at 18 GeV supports this conclusion. The comparison further indicates that the largest violations of scaling occur in the "exotic" reaction $\gamma p \to K^- X$. The data are also analyzed according to the triple Regge model of inclusive reactions and the effective trajectories have been determined.

1. Introduction

Inclusive reactions of the type $a + b \to c + X$ have lately been given much attention both experimentally and theoretically [1]. Such an inclusive reaction is a quasi two body process and the kinematics is therefore completely determined by the momentum $\boldsymbol{p}$ and the mass m of the detected particle c together with s, the total center of mass energy squared. In terms of these variables the Lorentz invariant cross section $d^3\sigma$ can be written as:

$$d^3\sigma = (d^3p/E) f(\boldsymbol{p}, s),$$

where in general the structure function $f(\boldsymbol{p}, s)$ is a function of both $\boldsymbol{p}$ and s. Many models [2], however, predict a particularly simple behaviour for $f(\boldsymbol{p}, s)$ at high energies. These predictions, known as scaling or limiting fragmentation, have been tested over a wide range in energies and secondary momenta in reactions involving only hadrons. In photoproduction, however, only a few inclusive experiments have been

carried out so far. The reaction $\gamma p \to \pi^- X$ has been investigated at SLAC for photon energies between 2.8 and 15 GeV [3]. Pion inclusive spectra (as well as ρ° and Δ^{++} distributions) were measured at 7.5 GeV in the reaction $\gamma d \to \pi^- X$ [4]. Preliminary data on $\gamma p \to \pi^\pm X$ and $\gamma p \to K^\pm X$ at 18 GeV were presented at the 1971 Cornell Conference [5]. Also available are preliminary data on $\gamma p \to \pi^\pm X$ and $\gamma p \to pX$ from a streamer chamber experiment at DESY [6]. Recently also the reaction $\gamma p \to \pi^0 X$ has been measured [7] at a photon energy of 6 GeV.

The photoproduction data and the hadron data, normalized to the respective total cross sections, show similar behaviour (limited transverse momentum, leading particle effects etc.) indicating that a photon behaves like a hadron in inclusive reactions like it seems to do in two body reactions, That is, we can use the photon just as another particle to investigate scaling and limiting behaviour. In particular, an incident photon beam is well suited for investigating scaling in the projectile fragmentation region. If the photon induced inclusive reactions have reaced the scaling limit, then it follows from C-invariance that the π^+/π^- and K^+/K^- ratios should be equal to one in the photon fragmentation region [8–10]. The scaling behaviour can therefore be tested by a measurement of the particle-antiparticle yield at a single energy.

The preliminary SLAC data [5] at 18 GeV show that the ratio π^+/π^- is indeed approaching one, whereas the K^+/K^- ratio is much larger than one in this region. These results indicate that the reactions $\gamma p \to \pi^\pm X$ may have approached the scaling limit at 18 GeV whereas at least one of the reactions $\gamma p \to K^\pm X$ has not yet reached the scaling limit at this energy.

In this paper we report the results of a measurement of the reactions $\gamma p \to \pi^\pm X$, $\gamma p \to K^\pm X$ and $\gamma p \to pX$ in the photon fragmention region[+]. The experiment was carried out at DESY and data were taken for transverse momenta between 0.3 GeV/c and 1.0 GeV/c at an average photon energy of 6 GeV. From the data we have determined the invariant cross sections as a function of longitudinal and transverse momentum and compared them directly to existing data. Furthermore, using the measured π^+/π^- and K^+/K^- ratios, we have investigated scaling as a function of transverse momentum. The data has also been analyzed using the triple Regge model and the effective trajectories have been determined.

2. Experimental method

The layout of the experiment is shown in fig. 1. A bremsstrahlung beam with a typical intensity of 8×10^{10} equivalent quanta per second was passed through a 27.8 cm long hydrogen target and was monitored with a quantameter. The calibration of the quantameter was frequently checked using a calorimeter. The angle θ

[+] Preliminary results of this experiment have been submitted to the 1972 Int. Conf. on high energy physics, Batavia.

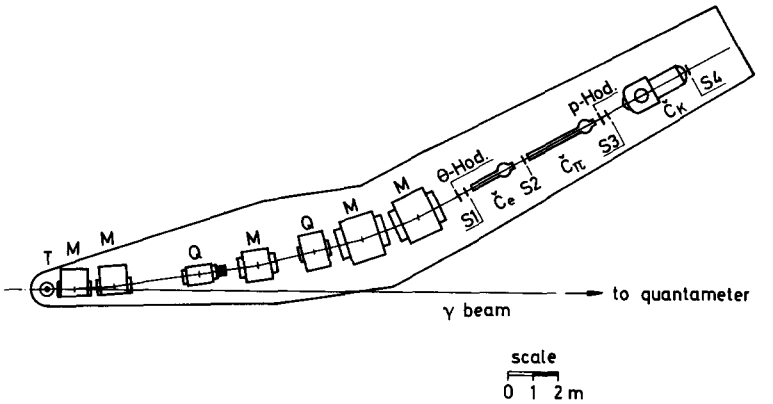

Fig. 1. Layout of the experiment. T liquid hydrogen target. M bending magnets. Q quadrupole magnets. S1, ... S4 scintillation counters. θ-Hod., p-Hod. Hodoscopes. C_e, C_π, C_K Cerenkov counters.

and the momentum p of the produced particles were determined using a focussing magnetic spectrometer. The spectrometer accepted ± 10 mrad in the production angle and had a total acceptance $(\Delta p/p)\,\Delta\Omega$ of 17.6×10^{-6} sterad. The acceptance was subdivided into 26 bins in Δp and 20 bins in $\Delta\theta$ by hodoscope counters located in the focal planes of the spectrometer.

The particles were identified using two threshold Cerenkov counters C_e and C_π set to respond respectively to electrons (positrons) and pions, and a differential Cerenkov counter C_K responding to kaons. Due to the high trigger rates the data were in general not analyzed event by event using the on-line computer but rather fed directly to fast scalers. However, to ensure the proper operation of the apparatus, a small subsample was written on tape and analyzed on-line.

In order to measure the cross sections at a definite photon energy, bremsstrahlung beams with endpoint energies of 6.5 GeV and 5.5 GeV were used and the yields for a fixed spectrometer momentum and angle were subtracted. The resulting yield is then mainly due to photons with energies between the two endpoint energies with a small contribution from photons at lower energies. Also the corresponding empty target rate was determined for each yield point. To minimize systematic errors the endpoint energies were switched frequently and as a check the yields at a fixed kinematical point were measured periodically during the course of the whole experiment.

The raw data were corrected for Cerenkov counter inefficiencies, nuclear absorption, decay in flight and for the contribution from photons with energies below 5.5 GeV. The kaon Cerenkov counter was (95 ± 1)% efficient, the pion counter more than 99.8%. The correction due to nuclear absorption was rather large (25%–40%) since the particles had to traverse the high pressure (15 to 20 atm) kaon Cerenkov counter filled with Freon-13. The particle loss was determined experimentally for the pions and protons. From these measurements the loss of kaons was

computed using the ratios of the absorption cross sections for pions and kaons on Freon, derived from a Woods-Saxon potential [11]. The uncertainty in the cross section due to the nuclear absorption correction was 2–3% for the pions, 6–8% for the kaons and 3–5% for the protons. The decay correction was quite serious for the kaons. At 2.5 GeV/c, 75% decayed before reaching the last counter. The effective decay length, however, was very well known since a kaon which decayed in front of the C_K counter was not identified as a kaon. In the case that the decay muon traversed the counter system it was either vetoed by the C_π counter or not registered by the differential C_K counter. The decay length was therefore known to be (25.5 ± 0.5)m leading to an uncertainty in the kaon cross sections of ± 3%. For the pions, the decay loss was between (5 ± 1.5)% and (11 ± 2)%.

The contribution to the particle yields from photons with energies below 5.5 GeV was computed assuming scaling for the cross sections. The correction was found to be between −3% and +5%. (A negative contribution may arise since subtracting a bremsstrahlung spectrum of 5.5 GeV maximum energy from a spectrum of 6.5 GeV maximum energy leads to a negative number of photons in the energy range 4.8–5.5 GeV). A systematic error of ± 1.5% is assigned to the cross sections due to this correction. At $p_\perp = 0.3$ GeV/c and $x = 0.53$ the correction was checked experimentally by lowering the maximum bremsstrahlung energy from 6.5 to 3.0 GeV in steps of 0.5 GeV.

From comparing a selected yield point at various times we found that the rates were reproduced to better than ± 1% during the course of the whole experiment. The short time reproducibility is conservatively assumed to be also ± 1%. At low secondary momenta where the rates from the two endpoint energies become similar, this might introduce an error of up to 10%, but for most of the data points the error is only about 2%.

The errors caused by the various corrections and uncertainties and the statistical error were added quadratically and this is the error quoted in the tables and figures. In addition there is an estimated normalization uncertainty of ± 7% from quantameter calibration, spectrometer acceptance and hydrogen target thickness.

3. The data

The kinematic region covered in this experiment is depicted in fig. 2 where the location of the pion data is shown as a function of transverse momentum $p_\perp = p_{\text{lab}} \sin\theta_{\text{lab}}$ and $x = p_\parallel^{\text{cm}}/p_{\text{max}}^{\text{cm}}$.

The invariant cross sections $E\,\mathrm{d}^3\sigma/\mathrm{d}^3p = (E/p^2)\,\mathrm{d}^2\sigma/\mathrm{d}\Omega\,\mathrm{d}p$ for $\gamma p \to \pi^\pm X$, $\gamma p \to K^\pm X$ and $\gamma p \to pX$ are given in tables 1, 2, 3 as function of the variables $p_\perp$ and x. For convenience the values of p_{lab}, θ_{lab}, the rapidity $y = \frac{1}{2}\ln[(E+p_\parallel)/(E-p_\parallel)]$ the missing mass M_X and the four momentum transfer squared t between the photon and the detected particle are also listed. For $p_{\text{max}}^{\text{cm}}$, the maximum momentum of the outgoing hadron in the center of mass frame was chosen, that is, $p_{\text{max}}^{\text{cm}}$ is the

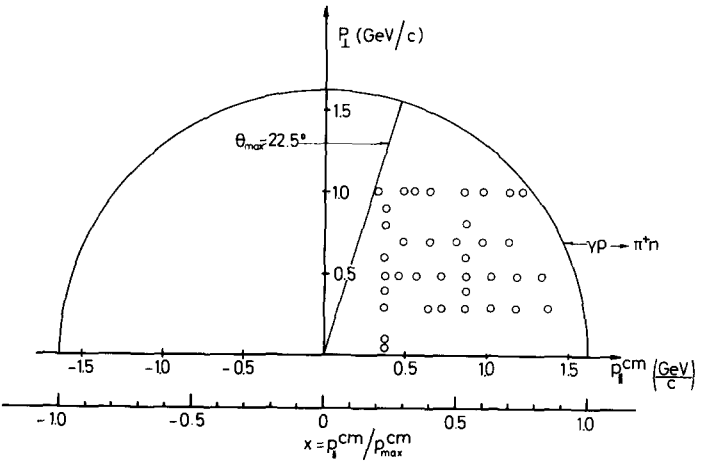

Fig. 2. Location of the data points for $\gamma p \to \pi^+ X$ as a function of the longitudinal and transverse momentum in the center of mass system.

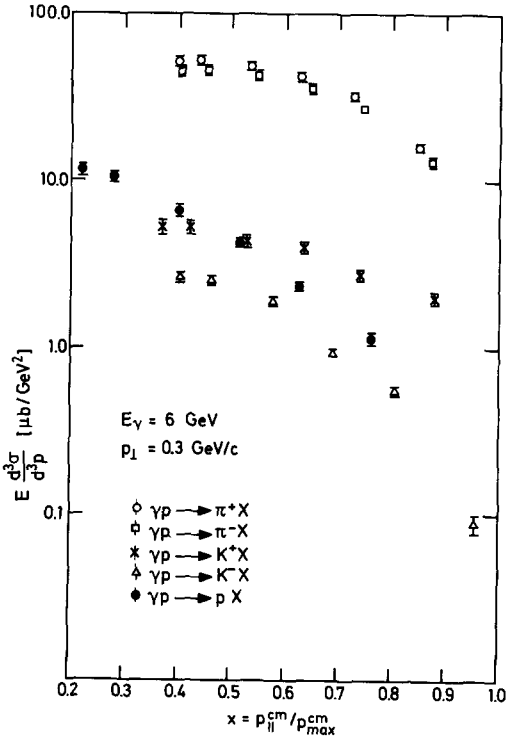

Fig. 3. Invariant cross sections for pion, kaon and proton production at a transverse momentum of 0.3 GeV/c, plotted *versus* $x = p_{\parallel}^{cm}/p_{max}^{cm}$.

Table 1:

$E\frac{d^3\sigma}{d^3p}$ [μb/GeV^2] for $\gamma p \to \pi^{\pm} X$ at 6 GeV

$p_\perp$ GeV/c	p_{lab} GeV/c	θ_{lab} deg	x_{π^+}	$\left(E\frac{d^3\sigma}{d^3p}\right)_{\pi^+}$	x_{π^-}	$\left(E\frac{d^3\sigma}{d^3p}\right)_{\pi^-}$	y_{lab}	M_X GeV/c^2	$-t$ (GeV/c)^2
0.06	1.45	2.40	0.23	119.8 ± 12.7	0.24	109.7 ± 10.75	2.94	3.06	0.07
0.1	1.45	3.96	0.23	107.6 ± 11.3	0.24	96.4 ± 10.9	2.83	3.05	0.10
	1.63	10.64	0.23	73.7 ± 5.8	0.24	59.9 ± 4.9	2.28	2.95	0.39
	2.54	6.79	0.40	51.3 ± 3.2	0.41	45.3 ± 2.6	2.73	2.67	0.24
	2.80	6.16	0.44	52.8 ± 2.8	0.46	46.2 ± 2.2	2.83	2.58	0.22
0.3	3.33	5.16	0.53	48.8 ± 1.8	0.55	43.0 ± 1.5	3.00	2.39	0.18
	3.89	4.43	0.63	42.0 ± 1.1	0.65	35.7 ± 0.87	3.16	2.10	0.15
	4.45	3.87	0.73	32.5 ± 0.58	0.75	27.1 ± 0.50	3.29	1.91	0.12
	5.18	*3.32*	*0.85*	*16.0 ± 0.44*	*0.87*	*13.1 ± 0.35*	3.44	*1.52*	*0.11*
	1.76	13.16	0.23	48.1 ± 3.58	0.24	35.0 ± 2.68	2.10	2.87	0.60
0.4	3.40	6.75	0.53	33.3 ± 1.06	0.55	27.6 ± 0.82	2.77	2.34	0.30
	1.39	21.00	0.11	25.5 ± 1.60	0.11	13.8 ± 2.0	1.65	2.89	1.18
	1.87	15.50	0.22	21.0 ± 1.85	0.23	15.6 ± 1.2	1.96	2.79	0.86
	2.14	13.50	0.28	21.6 ± 1.61	0.29	16.4 ± 1.1	2.10	2.71	0.75
	2.49	11.60	0.35	20.6 ± 1.30	0.36	15.6 ± 0.88	2.25	2.61	0.64
0.5	2.97	9.68	0.44	20.4 ± 0.90	0.45	16.0 ± 0.62	2.43	2.46	0.52
	3.49	8.24	0.53	19.1 ± 0.61	0.55	14.6 ± 0.39	2.59	2.27	0.45
	4.02	7.14	0.63	14.8 ± 0.42	0.65	11.2 ± 0.23	2.74	2.05	0.38
	4.57	6.28	0.73	10.4 ± 0.20	0.75	6.86 ± 0.11	2.87	1.79	0.34
	5.13	5.59	0.82	5.92 ± 0.18	0.85	4.06 ± 0.05	2.98	1.49	0.30
	2.07	16.87	0.23	11.4 ± 0.92	0.24	8.65 ± 0.58	1.83	2.67	1.10
0.6	3.59	9.62	0.53	10.0 ± 0.32	0.54	6.65 ± 0.17	2.45	2.18	0.62
	2.55	15.94	0.30	5.74 ± 0.40	0.31	4.11 ± 0.21	1.49	2.48	1.16
	3.03	13.37	0.40	5.43 ± 0.27	0.41	3.64 ± 0.15	2.13	2.33	1.00
0.7	3.54	11.42	0.50	4.87 ± 0.18	0.51	3.14 ± 0.09	2.28	2.16	0.85
	4.06	9.92	0.60	4.22 ± 0.12	0.62	2.45 ± 0.06	2.43	1.94	0.74
	4.60	8.74	0.70	2.96 ± 0.16	0.72	1.35 ± 0.08	2.55	1.68	0.65

Table 1 (continued)

$E\frac{d^3\sigma}{d^3p}$ [μb/GeV^2] for $\gamma p \to \pi^{\pm} X$ at 6 GeV

	2.41	19.35	0.23	2.91 ± 0.23	0.24	1.92 ± 0.14	1.76	2.44	1.67
0.8	3.83	12.06	0.53	2.38 ± 0.08	0.55	1.35 ± 0.03	2.23	1.98	1.03
0.9	2.59	20.29	0.23	1.28 ± 0.12	0.24	0.90 ± 0.09	1.70	2.30	1.96
	2.66	22.05	0.20	0.541 ± 0.048	0.20	0.416 ± 0.033	1.63	2.18	2.33
	3.06	19.06	0.30	0.558 ± 0.032	0.31	0.429 ± 0.024	1.78	2.09	2.00
1.0	3.21	18.10	0.34	0.565 ± 0.026	0.35	0.408 ± 0.014	1.82	2.04	1.93
	3.50	16.61	0.40	0.558 ± 0.029	0.41	0.360 ± 0.017	1.91	1.95	1.76
	4.10	14.10	0.53	0.553 ± 0.017	0.54	0.260 ± 0.007	2.08	1.71	1.49
	4.46	12.97	0.60	0.481 ± 0.034	0.62	0.193 ± 0.021	2.17	1.55	1.37
	4.97	11.62	0.70	0.291 ± 0.028	0.72	0.192 ± 0.009	2.28	1.26	1.23
	5.23	11.03	0.75	0.431 ± 0.019	0.77	0.060 ± 0.026	2.33	1.08	1.16

$p_{max}^{cm} = 1.612$ GeV/c for π^+, $p_{max}^{cm} = 1.572$ GeV/c for π^-

Table 2:

$E\frac{d^3\sigma}{d^3p}$ [μb/GeV^2] for $\gamma p \to K^{\pm} X$ at 6 GeV

$p_\perp$ GeV/c	p_{lab} GeV/c	θ_{lab}	x_{K^+}	$\left(E\frac{d^3\sigma}{d^3p}\right)_{K^+}$	x_{K^-}	$\left(E\frac{d^3\sigma}{d^3p}\right)_{K^-}$	y_{lab}	M_X GeV	$-t$ GeV/c^2
	2.54	6.79	0.37	5.24 ± 0.46	0.40	2.61 ± 0.16	2.18	2.60	0.54
	2.80	6.16	0.43	5.26 ± 0.40	0.46	2.54 ± 0.13	2.28	2.52	0.47
	3.33	5.17	0.53	4.35 ± 0.31	0.58	1.89 ± 0.08	2.45	2.34	0.36
0.3	3.89	4.43	0.64	3.97 ± 0.23	0.69	0.938 ± 0.041	2.60	2.13	0.27
	4.45	3.87	0.74	2.79 ± 0.10	0.81	0.550 ± 0.022	2.74	1.88	0.21
	5.18	3.32	0.88	2.01 ± 0.15	0.96	0.088 ± 0.011	2.89	1.50	0.14

Table 2: (continued)

$E\frac{d^3\sigma}{d^3p}$ [μb/GeV^2] for $\gamma p \to K^{\pm}X$ at 6 GeV

0.4	3.40	6.75	0.53	3.38 ± 0.20	0.58	1.20 ± 0.06	2.37	2.29	0.47
	1.87	15.50	0.17	2.50 ± 0.79	0.19	0.855 ± 0.193	1.67	2.68	1.34
	2.14	13.50	0.24	2.70 ± 0.54	0.26	1.05 ± 0.16	1.81	2.62	1.14
	2.49	11.60	0.31	2.91 ± 0.27	0.35	1.12 ± 0.08	1.96	2.54	0.95
0.5	2.97	9.68	0.42	2.85 ± 0.22	0.46	0.882 ± 0.048	2.14	2.39	0.75
	3.49	8.24	0.53	2.74 ± 0.19	0.58	0.623 ± 0.032	2.30	2.22	0.61
	4.02	7.14	0.64	2.49 ± 0.19	0.69	0.458 ± 0.023	2.44	2.01	0.49
	4.57	6.28	0.74	1.95 ± 0.08	0.81	0.212 ± 0.009	2.57	1.76	0.40
	5.13	5.59	0.85	1.73 ± 0.09	0.93	0.051 ± 0.005	2.68	1.46	0.33
0.6	3.59	9.62	0.53	1.86 ± 0.13	0.58	0.374 ± 0.020	2.22	2.14	0.77
	2.55	15.94	0.27	0.71 ± 0.17	0.29	0.266 ± 0.041	1.77	2.40	1.50
	3.03	13.37	0.38	1.10 ± 0.15	0.42	0.314 ± 0.031	1.95	2.27	1.22
0.7	3.53	11.42	0.50	1.14 ± 0.09	0.54	0.234 ± 0.016	2.11	2.11	1.01
	4.06	9.91	0.61	1.05 ± 0.06	0.66	0.139 ± 0.008	2.25	1.90	0.84
	4.61	8.74	0.72	1.06 ± 0.10	0.78	0.043 ± 0.009	2.37	1.65	0.71
0.8	3.83	12.06	0.53	0.62 ± 0.05	0.58	0.092 ± 0.006	2.09	1.94	1.15
	2.66	22.05	0.17	0.119 ± 0.028	0.18	0.045 ± 0.009	1.54	2.10	2.64
	3.06	19.06	0.28	0.141 ± 0.018	0.30	0.038 ± 0.005	1.68	2.02	2.25
1.0	3.22	18.10	0.32	0.125 ± 0.012	0.35	0.029 ± 0.003	1.73	1.98	2.13
	3.50	16.61	0.39	0.150 ± 0.017	0.42	0.0173 ± 0.004	1.82	1.89	1.92
	4.10	14.10	0.53	0.167 ± 0.009	0.58	0.0115 ± 0.001	1.98	1.67	1.60
	4.46	12.97	0.61	0.160 ± 0.020	0.66	0.0051 ± 0.002	2.07	1.52	1.45
	4.97	11.62	0.72	0.173 ± 0.016			2.18	1.23	1.27

p^{cm}_{max} = 1.520 GeV/c for K^+, p^{cm}_{max} = 1.398 GeV/c for K^-

Table 3:

$E\frac{d^3\sigma}{d^3p}$ [μb/GeV^2] for $\gamma p \to pX$ at 6 GeV

$p_\perp$ GeV/c	p_{lab} GeV/c	θ_{lab}	x	$E\frac{d^3\sigma}{dp^3}$ $\frac{\mu b}{GeV^2}$	y_{lab}	M_X GeV	$-t$ (GeV/c)^2
	2.54	6.79	0.22	11.45 ± 0.80	1.67	2.39	1.35
	2.80	6.16	0.28	10.43 ± 0.56	1.76	2.34	1.15
0.3	3.33	5.17	0.40	6.63 ± 0.41	1.93	2.19	0.84
	3.89	4.43	0.51	4.25 ± 0.18	2.08	2.01	0.60
	4.45	3.87	0.63	2.35 ± 0.07	2.21	1.79	0.42
	5.18	3.32	0.76	1.15 ± 0.10	2.36	1.43	0.23
0.4	3.40	6.75	0.40	5.60 ± 0.21	1.91	2.14	0.93
	2.49	11.60	0.17	8.36 ± 0.56	1.57	2.32	1.78
	2.97	9.68	0.29	5.91 ± 0.31	1.74	2.22	1.36
0.5	3.49	8.24	0.41	4.51 ± 0.18	1.89	2.08	1.04
	4.02	7.14	0.52	2.50 ± 0.13	2.03	1.90	0.79
	4.57	6.28	0.63	1.47 ± 0.050	2.16	1.68	0.59
	5.13	5.59	0.74	0.807 ± 0.051	2.27	1.38	0.43
0.6	3.59	9.62	0.41	2.91 ± 0.12	1.87	2.00	1.18
	2.55	15.94	0.13	4.29 ± 0.32	1.49	2.18	2.30
	3.03	13.37	0.25	2.88 ± 0.18	1.65	2.09	1.81
0.7	3.54	11.42	0.37	2.13 ± 0.09	1.81	1.96	1.43
	4.06	9.92	0.49	1.46 ± 0.05	1.94	1.73	1.13
	4.61	8.74	0.60	0.867 ± 0.07	2.07	1.56	0.90
0.8	3.83	12.06	0.41	1.19 ± 0.5	1.83	1.80	1.49
	2.66	22.05	0.03	0.828 ± 0.068	1.35	1.86	3.38
	3.06	19.06	0.15	0.620 ± 0.040	1.49	1.82	2.82
	3.22	18.10	0.20	0.577 ± 0.030	1.54	1.79	2.64
1.0	3.50	16.61	0.27	0.500 ± 0.028	1.63	1.73	2.36
	4.10	14.10	0.42	0.335 ± 0.013	1.79	1.54	1.88
	4.46	12.97	0.50	0.238 ± 0.026	1.87	1.39	1.66
	4.97	11.62	0.61	0.116 ± 0.020	1.98	1.12	1.39
	5.23	11.03	0.66	0.122 ± 0.013	2.03	0.95	1.29

p_{CM}^{max} = 1.616 GeV/c

center of mass momentum of the threshold reaction $\gamma p \to \pi^+ n$ for π^+, $\gamma p \to \pi^-(\pi^+ p)$ for π^-, $\gamma p \to K^+\Lambda$ for K^+, $\gamma p \to K^-(K^+ p)$ for K^- and $\gamma p \to \rho\gamma$ for p.

To display the gross features of the data we have plotted the invariant cross sections as a function of x at two different values of the transverse momentum. For a transverse momentum of 0.3 GeV/c, the invariant cross sections have been plotted *versus* x in fig. 3. The π^+, π^- and K^+ yields have nearly the same slowly varying x dependence at this value of $p_\perp$, whereas both the K^- and proton cross sections drop

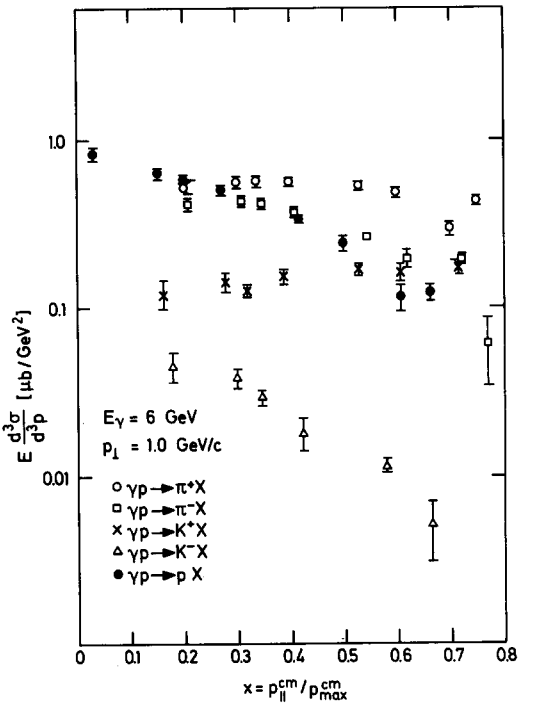

Fig. 4. Invariant cross sections at a transverse momentum of 1.0 GeV/c.

more steeply with increasing x. The π^+ cross section is about 10% larger than the π^- cross section and roughly an order of magnitude larger than the K^+ and proton cross sections. The K^+/K^--ratio is considerably larger than 1.

In fig. 4 the invariant cross sections are plotted *versus* x for a transverse momentum of 1 GeV/c. Note the rapid increase of the proton yield relative to the pion yield with transverse momentum. Also the K^+ yield has increased relative to the pion yield whereas the K^- yield is still only a few percent of the pion yield. The K^+ cross section is also fairly independent of x, in marked contrast to the K^- cross section. It is also worth noting that the π^+ cross section is now significantly larger than the π^- cross section.

4. Transverse momentum dependence

It is well known that the particle yields decrease rapidly with increasing transverse momentum. This is shown in fig. 5 where the invariant cross sections, at a fixed value of x, are plotted as function of the transverse momentum squared. The solid lines represent the results of a fit to the data of the form $A\ e^{-Bp_\perp^2}$. The kaon and the proton distributions are well represented by the fit for $p_\perp$ between 0.3 GeV/c

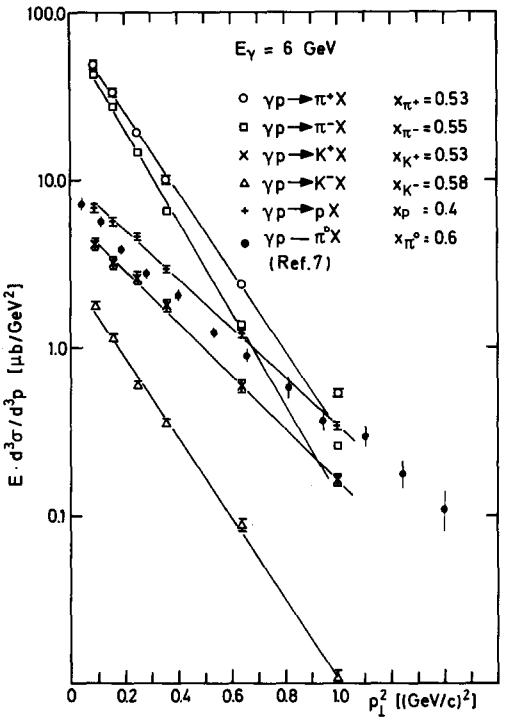

Fig. 5. $p_\perp^2$ dependence of inclusive photoproduction at fixed x. The solid lines are fits to the data of the form $A \exp(-B p_\perp^2)$.

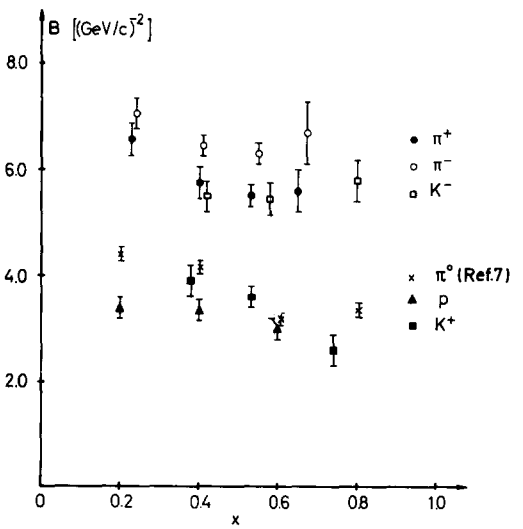

Fig. 6. The value of the slope parameter B determined from a fit of the form $A^{-Bp_\perp^2}$ (for $0.3 \leqslant p_\perp \leqslant 0.8$ GeV/c) is shown as a function of x.

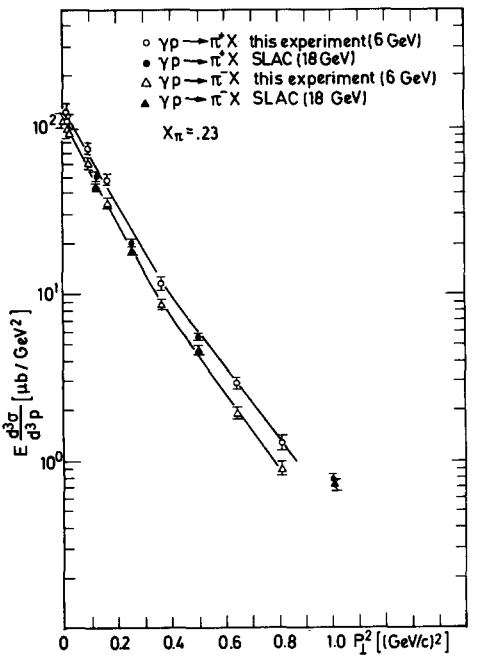

Fig. 7. Invariant cross section for $\gamma p \to \pi^{\pm} X$ as function of $p_\perp^2$ at $x = 0.23$. The solid lines are fits to the data of the form $A \exp(-B p_\perp^2)$. Fits were made for $p_\perp^2 \leqslant 0.35$ GeV^2 and $p_\perp^2 \geqslant 0.35$ GeV^2. Note the difference in slope for the two ranges in $p_\perp^2$. For comparison the preliminary 18 GeV SLAC data are shown.

and 1.0 GeV/c, whereas the pion distribution shows some deviations from this form at the largest value of $p_\perp$. It is evident from the fit that there is no universal slope for all particles, the pion and the K^- distributions have significantly steeper slopes than the proton and K^+ distributions. In fig. 6 the slope parameter B, determined for $p_\perp$ between 0.3 GeV/c and 0.8 GeV/c, is plotted as a function of x. For comparison, the slope values for the reaction $\gamma p \to \pi^0 X$ as determined in a recent experiment [7] are also included. In the x-range shown, the value of B clusters around $6(\text{GeV}/c)^{-2}$ for the π^+, π^- and the K^- distributions, whereas for the proton, the π^0 and the K^+ data B is around $4(\text{GeV}/c)^{-2}$. Hence the various values of B do not seem to be directly connected with the mass of the observed particle. It is also seen in this plot that B is not independent of x.

In fig. 7 the invariant cross sections for $\gamma p \to \pi^{\pm} X$ are plotted as a function of $p_\perp^2$ for $x \simeq 0.23$. For comparison the preliminary 18 GeV SLAC data are also shown. The agreement between the two sets of data is good for $\gamma p \to \pi^- X$, indicating that the transverse momentum distribution does not depend strongly on the energy. In the case of $\gamma p \to \pi^+ X$ the 6 GeV data seem to be systematically high with respect to the 18 GeV data.

5. The ratio of the particle and antiparticle yields

The Regge theory [8–10] of the inclusive reactions predicts that in the scaling limit the cross sections for the reactions $\gamma + p \to c + X$ and $\gamma + p \to \bar{c} + X$ should become equal in the photon fragmentation region. This follows from the observation that the Pomeranchuk trajectory is even under charge conjugation and that the photon couples to c and $\bar{c}$ with equal strength. Hence if we find experimentally that the yields of particles and antiparticles differ, then scaling must be violated. However, if we observe that the ratio is equal to one then the situation is more problematic, since any trajectory with positive charge conjugation will lead to a particle-antiparticle ratio of one. On the other hand, if besides the pomeron, secondary trajectories are important then it would be difficult to understand why only trajectories with $C = +1$ should contribute.

Experimentally a measurement of the particle ratios only involves changing the polarity of the spectrometer and it is therefore to a high degree free of systematic errors. In fig. 8 the π^+/π^- ratio is plotted *versus* x for various values of $p_\perp$. At $p_\perp$ = 0.3 GeV/c, this ratio is about 1.1 which indicates that scaling might be nearly valid for the bulk of the produced pions. At larger values of $p_\perp$, the π^+/π^- ratio increases,

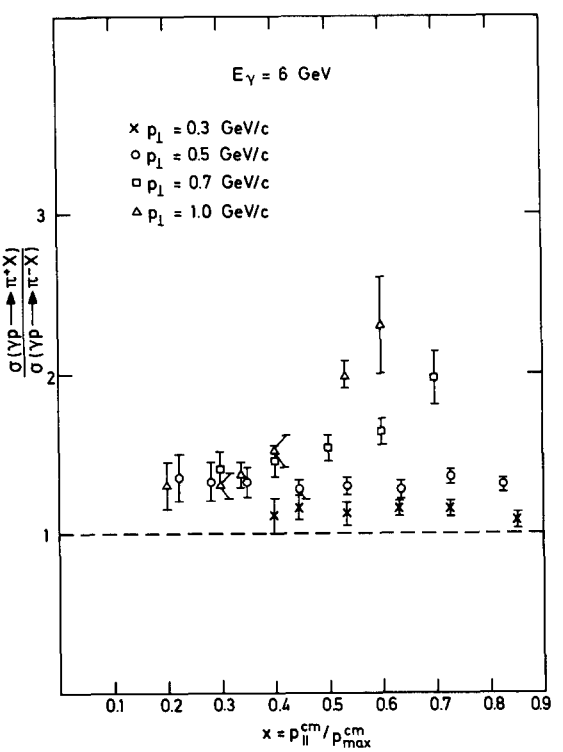

Fig. 8. Ratio of π^+ and π^- production *versus* x for various transverse momenta.

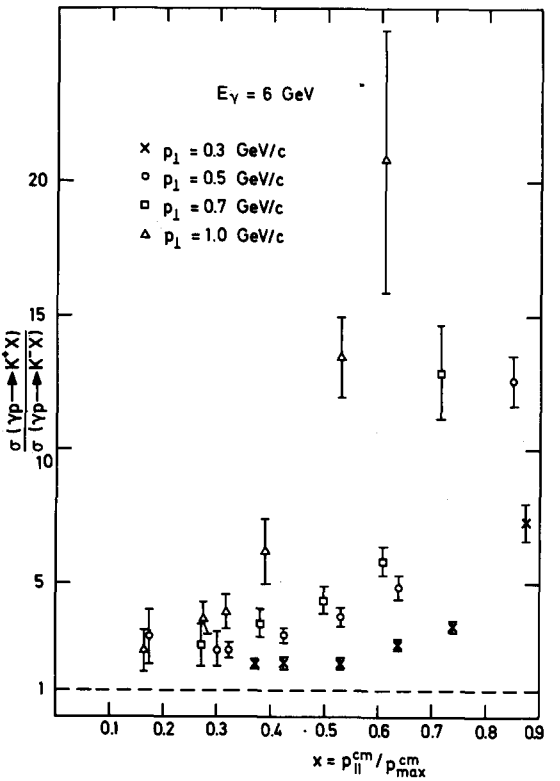

Fig. 9. Ratio of K^+ and K^- production *versus* x.

so scaling is certainly violated for at least one of the reactions $\gamma p \to \pi^+ X$ or $\gamma p \to \pi^- X$. Also note that the π^+/π^- ratio in general also increases with increasing values of x – i.e. with decreasing mass of the unobserved system X.

The K^+/K^- ratio is shown in fig. 9. Again the ratio increases with increasing values of $p_\perp$ and x. From this observation we conclude that scaling must be significantly violated in at least one of the K-production reactions.

These measurements seem to indicate that scaling is increasingly violated with increasing values of $p_\perp$. However, for fixed value of x, the missing mass of X is decreasing with increasing values of $p_\perp$, hence the apparent breakdown of scaling for larger values of $p_\perp$ could simply be due to low missing masses. This is supported by the preliminary results of the SLAC 18 GeV experiment [5]. At a fixed value of x the particle-antiparticle ratios observed in the SLAC experiment are significantly closer to one than the ratios observed in this experiment. That is, at fixed x the particle-antiparticle ratio seems to approach one with increasing values of the missing mass.

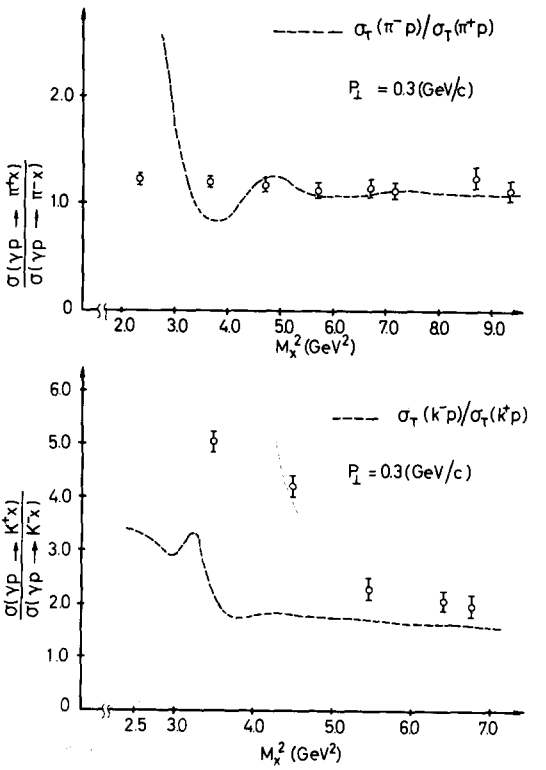

Fig. 10. π^+/π^- and K^+/K^- ratios for $p_\perp = 0.3$ GeV/c compared with predictions of the Drell model.

The ratio of the particle-antiparticle yields can be estimated from the Drell model [14]. This model predicts

$$\frac{\sigma(\gamma p \to \pi^+ X)}{\sigma(\sigma p \to \pi^- X)} = \frac{\sigma_T(\pi^- p)}{\sigma_T(\pi^+ p)} ,$$

and correspondingly

$$\frac{\sigma(\gamma p \to K^+ X)}{\sigma(\gamma p \to K^- X)} = \frac{\sigma_T(K^- p)}{\sigma_T(K^+ p)} .$$

Here σ_T denotes the total cross section evaluated at a center of mass energy equal to the mass of the unobserved system X. In fig. 10 the measured values for a transverse momentum $p_\perp = 0.3$ GeV/c are compared with the predicted values using the formula listed above. In the case of the pions the agreement is good for masses

above 2 GeV. In the case of the kaons there are some deviations at low missing masses, for higher missing masses, however, the measured values are only 20% above the predicted values.

6. Comparison with other experiments

The π^- data are compared in fig. 11 with data from the SLAC laser beam experiment [3] at 4.7 GeV and preliminary data at 18 GeV [5]. At transverse momenta of 0.3, 0.5 and 0.7 GeV/c the agreement between the different energies is fairly good indicating that scaling is nearly fulfilled in π^- production down to an energy of 4.7 GeV. At $p_\perp$ = 1.0 GeV/c however, where the cross section has dropped about two orders of magnitude, a sizable violation of scaling is seen. This is in agreement with the observation made from the π^+/π^- ratio of the 6 GeV data alone. The 6 GeV and the preliminary 18 GeV π^+ data are compatible with each other (see fig. 12), and so are the 6 and 18 GeV K^+ data (fig. 13). For K^- production, scaling may be approximately valid at $p_\perp \approx 0.5$ GeV/c but it is badly broken at $p_\perp$ =

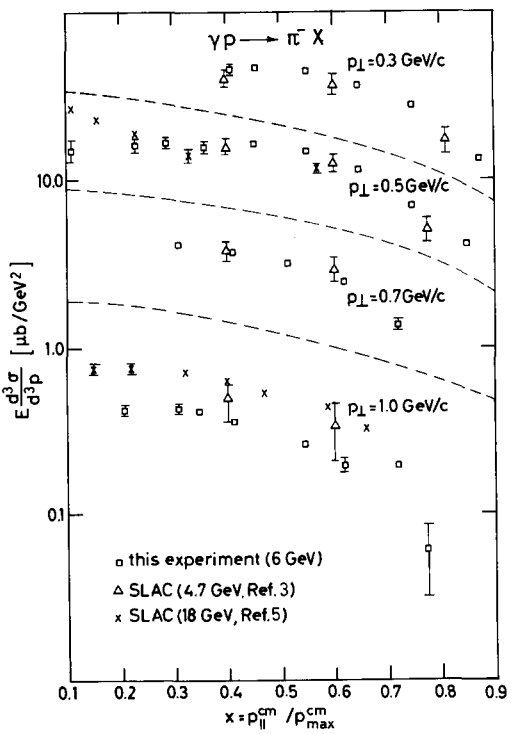

Fig. 11. Comparison of 4.7 GeV (ref. [3]), 6 GeV (this experiment) and preliminary 18 GeV (ref. [5]) data on $\gamma p \to \pi^- X$. Dotted lines are drawn to separate the data points for the various $p_\perp$ values.

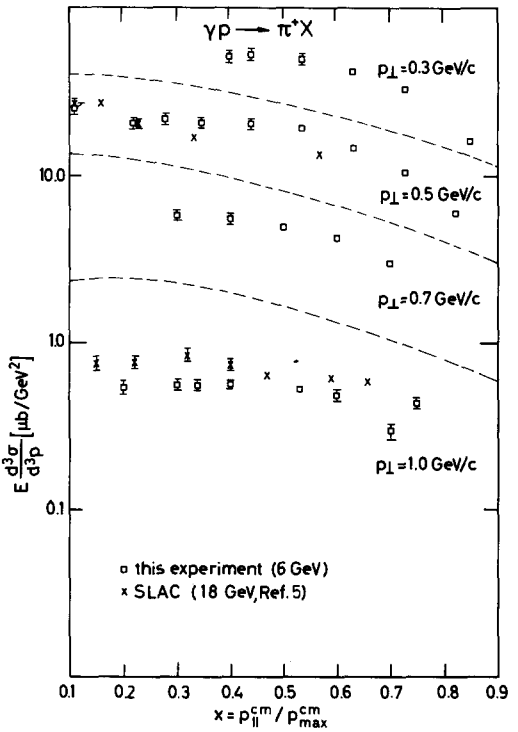

Fig. 12. Comparison of 6 GeV and 18 GeV data on $\gamma p \to \pi^+ X$.

1.0 GeV/c (fig. 14). K^- production seems to violate scaling more than the other observed reactions. This is in apparent diagreement with the conjecture [10] based on duality that if $(ab\bar{c})$ is exotic the reaction should scale at low energies in the fragmentation region.

For completeness, we show in fig. 15 the proton distribution at various transverse momenta although data at energies other than 6 GeV are not yet available.

7. Triple Regge analysis

Scaling and limiting behaviour can be derived in a Regge model using the observation by Mueller [8] that the total cross section for $a + b \to c + X$ is related to the elastic 3-body scattering amplitude $a + b + \bar{c}$.

Assuming the reaction to scale, Regge models [9, 10, 12, 13] predict the invariant cross section (for the particle c near its kinematic boundary) to be proportional to $(s/s')^{2\alpha(t)-1}$. In this formula s is the center of mass energy squared, s' is the missing mass squared, t is the square of the four momentum transfer between a and c, and $\alpha(t)$ represents the highest trajectory which can be exchanged

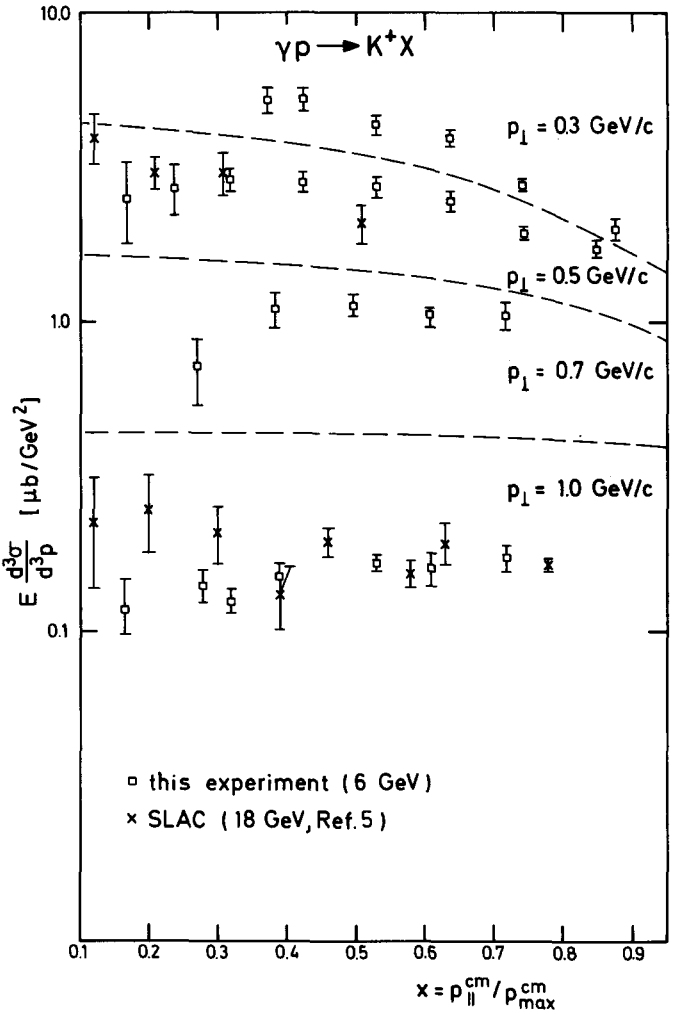

Fig. 13. Comparison of 6 GeV and 18 GeV data on $\gamma p \to K^+X$.

between the particle a and c. In the scaling limit $\alpha(t)$ can be either determined from measurements at fixed t and s', but various values of s, or from measurements at fixed t and s but various values of s'. Since the data were collected at only one incident energy the latter method was employed. Of course, in the scaling limit both methods should yield the same trajectory.

At the energy available to the experiment the conditions $s \gg s' \gg 1$, needed to derive the Regge expression, is not satisfied. Furthermore, the data show that the scaling limit is not yet reached at this energy. Hence, there must be corrections, resulting from the exchange of secondary trajectories or cuts, to the simple formula

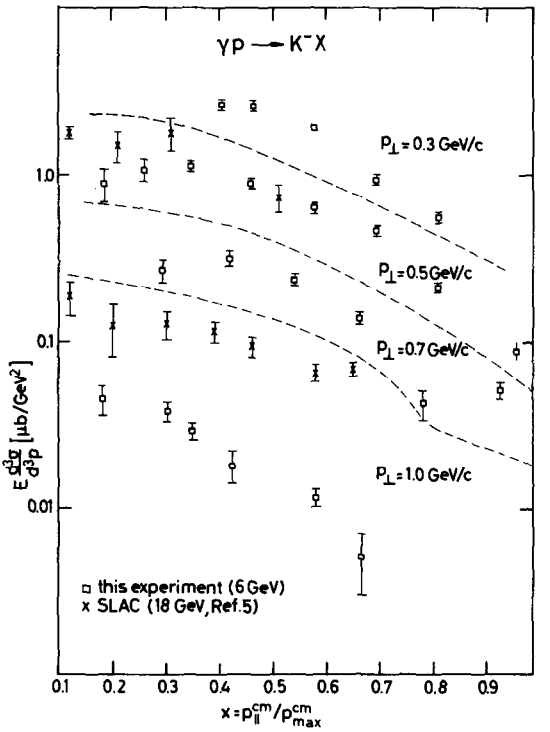

Fig. 14. Comparison of 6 GeV and 18 GeV data on $\gamma p \to K^- X$.

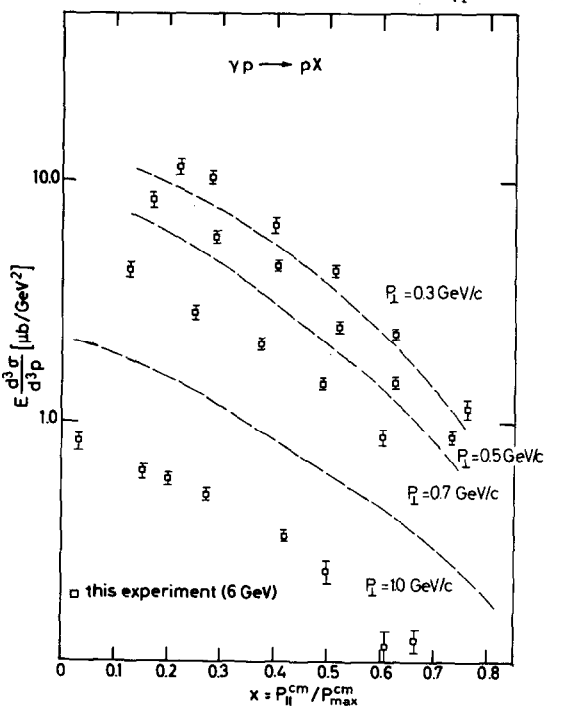

Fig. 15. $\gamma p \to pX$ at 6 GeV for various transverse momenta.

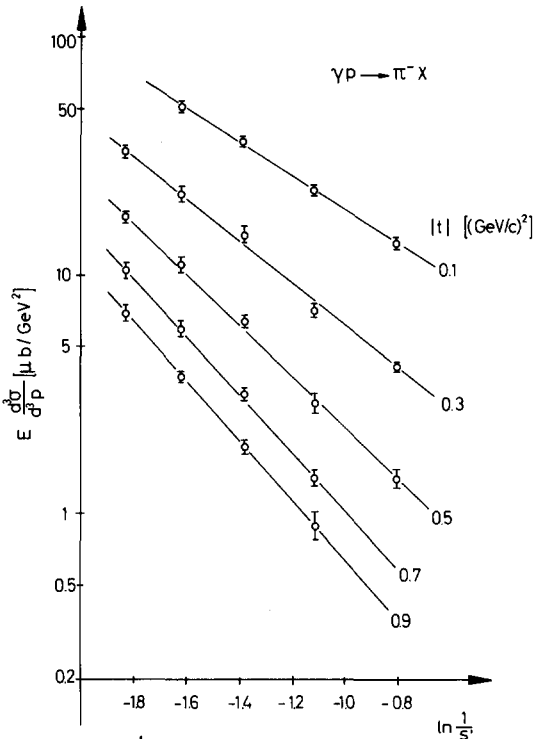

Fig. 16. Invariant cross section for π^+ production at various momentum transfers are plotted versus ln $(1/s')$ ($s' = M_X^2$ missing mass squared).

given above. However, if the cross section is proportional to some power $(s/s')^{n(t)}$ it is still possible to determine an effective trajectory for the process.

By interpolating between data points the invariant cross section for $\gamma p \to \pi^- X$ has been plotted in fig. 16 as a function of ln $(1/s')$ for various values of t. It is clear from the plot that the data are well represented by a straight line as expected from the Regge model. The same plot has also been made for the other reactions studied. With the exception of $\gamma p \to pX$, these plots confirm that the energy dependence of the invariant cross sections is indeed well described by the form $(s/s')^{n(t)}$.

From the plots above the effective trajectory $\alpha(t)$ can be determined. The effective trajectory for the reactions $\gamma p \to \pi^{\pm} X$ is shown in fig. 17a and fig. 17b. The trajectories so determined tend to flatten out at larger values of $|t|$. In contrast to the behaviour observed in two body photoproduction processes, the inclusive pion cross sections show shrinkage. Also note that the effective trajectory is well below the ρ and A_2 trajectories and in rough agreement with the pion trajectory. In fig. 17c the effective trajectories for $\gamma p \to K^{\pm} X$ are plotted *versus t*. The effective trajectory for $\gamma p \to K^+ X$ has a slope of about 0.5 $(\mathrm{GeV}/c)^{-2}$ whereas the effective trajectory for the exotic reaction $\gamma p \to K^- X$ is flat within the large incertainties and well below the other trajectories.

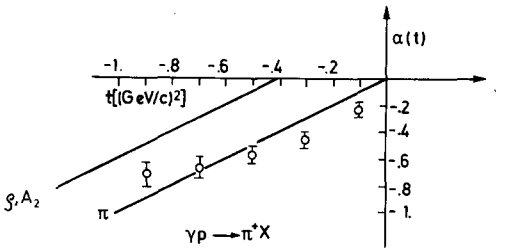

fig. 17a.

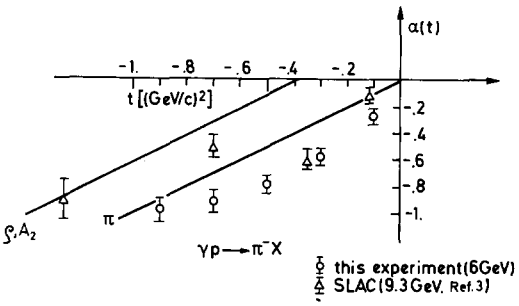

Fig. 17b.

Fig. 17(a) The effective trajectory for the reaction $\gamma p \to \pi^+ X$ is shown. For comparison the "π trajectory" is also plotted. (b) The effective trajectory for $\gamma p \to \pi^- X$. Points determined from the SLAC data at 9.3 GeV (ref. [3]) are also shown.

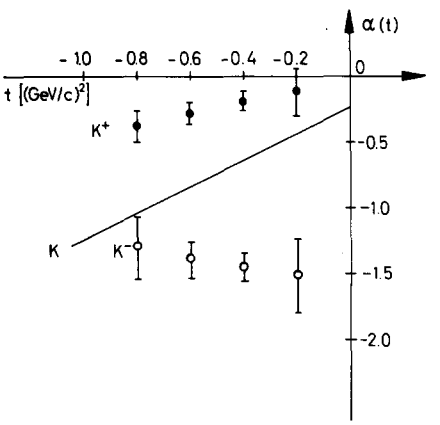

Fig. 17. (c) The effective trajectories for $\gamma p \to K^+ X$, $\gamma p \to K^- X$.

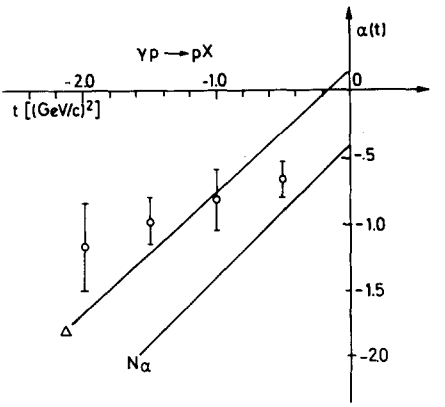

Fig. 17. (d) The effective trajectory for $\gamma p \to pX$.

The effective trajectory for $\gamma p \to pX$ is shown in fig. 17d. Here the error bars have been increased to account for the observed deviations from a power law.

References

[1] E.L. Berger, ANL/HEP 7148;
W. Frazer, L. Ingber, C.H. Mehta, C.H. Poon, D. Silverman, K. Stowe, P.D. Ting and H.J. Yesian, Rev. Mod. Phys. 44 (1972) 284;
L. Van Hove, Phys. Reports 1 (1971) 347;
D. Horn, Phys. Reports 4 (1972) 1.

[2] R.P. Feynmann, Phys. Rev. Letters 23 (1969) 1415;
J. Benecke, T.T. Chou, C.N. Yang and E. Yen, Phys. Rev. 188 (1969) 2159.

[3] K.C. Moffeit, J. Ballam, G.B. Chadwick, M. Della-Negra, R. Gearhart, J.J. Murray, P. Seyboth, C.K. Sinclair, I.O. Skillicorn, H. Spitzer, G. Wolf, H.H. Bingham, W.B. Fretter, W.J. Podolsky, M.S. Rabin, A.H. Rosenfeld, R. Windmolders, G.P. Yost and R.H. Milburn, Phys. Rev. D5 (1972) 1603;
W.P. Swanson, M. Davier, I. Derado, D.C. Fries, F.F. Liu, R.F. Mozley, A.C. Odian, J. Park, F. Villa and D.E. Yount, Phys. Rev. Letters 27 (1971) 1472.

[4] G. Alexander, O. Benary, S. Dagan, J. Gandsman, J. Grunhaus, P. Katz, A. Levy and D.A. Lissauer, Phys. Rev. D8 (1973) 712;
J. Gandsman, G. Alexander, S. Dagan, L.D. Jacobs, A. Levy, D. Lissauer and L. M. Rosenstein, Tel Aviv University preprint TAUP-360-73.

[5] A.M. Boyarski, D. Coward, S. Ecklund, B. Richter, D. Sherden, R. Siemann and C. Sinclair, Paper submitted to the Int. Symposium on electron and photon interactions at high energies 1971, Cornell University, Ithaca, N.Y.

[6] W. Struczinski, P. Dittmann, V. Eckardt, P. Joos, A. Ladage, H. Meyer, B. Naroska, D. Notz, S. Yellin, G. Hentschel, J. Knobloch, E. Rabe, S. Brandt, M. Grimm, D. Pollmann, I. Derado, R. Meinke, P. Schacht, H. Strobl and P. Söding, Paper 668 submitted to the 16th Int. Conf. on high energy physics, Chicago, Batavia, 1972.

[7] Ch. Berger, G. Dick, W. Erlewein, K. Lübelsmeyer, L. Paul, H. Meyer-Wachsmuth and A. Schultz von Dratzig, DESY report 73/43.

[8] A.H. Mueller, Phys. Rev. D2 (1970) 2963.

[9] H.D.I. Abarbanel, Phys. Letters 34B (1971) 69.

[10] Chan Hong-Mo, C.S. Hsue, C. Quigg and Jiunn-Ming Wang, Phys. Rev. Letters 26 (1971) 672.

[11] K.C. Stanfield, private communication.

[12] Min-Shih Chen, Ling-Lie Wang and T.F. Wong, Phys. Rev. D5 (1972) 1667.

[13] N.S. Craigie, G. Kramer and J. Körner, Nucl. Phys. B68 (1974) 509.

[14] S.D. Drell, Phys. Rev. Letters 5 (1960) 278.